INSTITUTE OF PHYSICS PUBLISHING JOURNAL OF PHYSICS B: ATOMIC, MOLECULAR AND OPTICAL PHYSICS

J. Phys. B: At. Mol. Opt. Phys. **36** (2003) 173–196 PII: S0953-4075(03)36915-9

Electron impact excitation of H_2: resonance excitation of B $^1\Sigma_u^+(J_j = 2, v_j = 0)$ and effective excitation function of EF $^1\Sigma_g^+$

Xianming Liu[1], D E Shemansky[1], H Abgrall[2], E Roueff[2], S M Ahmed[3,4] and J M Ajello[3]

[1] Department of Aerospace and Mechanical Engineering, University of Southern California, Los Angeles, CA 90089, USA
[2] Observatoire de Paris, Section de Meudon, DAEC and CNRS UMR 8631, 92195 Meudon Cedex, France
[3] Jet Propulsion Laboratory, California Institute of Technology, 4800 Oak Grove Drive, Pasadena, CA 91109, USA

E-mail: xianming@usc.edu, dons@hippolyta.usc.edu, abgrall@mesioc.obspm.fr, evelyne.roueff@obspm.fr, ahmed@ipr.res.in and jajello@pop.jpl.nasa.gov

Received 3 May 2002, in final form 19 November 2002
Published 7 January 2003
Online at stacks.iop.org/JPhysB/36/173

Abstract

The electron impact emission function of the P(3) branch for the (0, 4) band of the H_2 B $^1\Sigma_u^+$–X $^1\Sigma_g^+$ band system has been measured from threshold to 1800 eV. The emission function exhibits structure indicating strong contributions from both resonance and non-resonance excitation. The non-resonance component contains direct and cascade contributions. A combination of experimental and theoretical considerations permits separation of resonance, dipole-allowed direct, dipole-allowed indirect, and dipole-forbidden excitation components for the $J_j = 2$, $v_j = 0$ level of the B $^1\Sigma_u^+$ state. An effective excitation function for the EF $^1\Sigma_g^+$–X $^1\Sigma_g^+$ band system has been obtained from a nonlinear least-squares analysis of the dipole-forbidden component of the B $^1\Sigma_u^+$ state emission function. The absolute value of EF $^1\Sigma_g^+$–X $^1\Sigma_g^+$ cross section is established on the basis of earlier experimental results of Liu *et al* 1995 *Astrophys. J. Suppl.* **101** 375–99 and 2002 *Astrophys J. Suppl.* **138** 229–45 and Abgrall *et al* 1997 *Astrophys. J.* **481** 557–66 and 1999 *J. Phys. B: At. Mol. Opt. Phys.* **32** 3813–38. A near-threshold apparent resonance excitation cross section of $(8.1 \pm 3.2) \times 10^{-18}$ cm^2 is obtained for the B $^1\Sigma_u^+$ ($J_j = 2$ and $v_j = 0$). An EF $^1\Sigma_g^+$–X $^1\Sigma_g^+$ Born cross section has been calculated from the electronic form factor of Kolos *et al* 1982a *J. Chem. Phys.* **77** 1335–44. Analysis shows that the Born asymptotic shape function of the EF $^1\Sigma_g^+$–X $^1\Sigma_g^+$ band system starts at ∼400 eV, a significantly higher energy than previously expected. The excitation function is especially important for interpreting outer planet

[4] Present address: Institute for Plasma Research, Gandhinagar, India.

0953-4075/03/020173+24$30.00

atmospheric dayglow and auroral activity and can be used to infer energy deposition and heating rates.

1. Introduction

Electron impact excitation of molecular hydrogen is an important excitation mechanism in molecular clouds and atmospheres of outer planets. A number of spacecraft observations of the dayglow and auroral activity in the outer planet atmospheres have indicated an emission spectrum characteristic of low-energy electron impact excitation of molecular hydrogen (Pryor *et al* 1998, Ajello *et al* 1998, 2001, Ingersoll *et al* 1998, Vasavada *et al* 1999). Reliable excitation functions and accurate cross sections, especially in the low-energy region, are vital for the determination of excitation conditions.

Electron impact excitation in the high-energy region is formally equivalent to photon excitation from a white uniform radiation field. In the low-energy region, however, both dipole (and spin) forbidden and resonance excitations are possible. Near threshold, both forbidden and resonance excitations can be comparable to, or stronger than, allowed excitation. Resonance excitation of excited electronic states of H_2 typically takes place between 11 and 16 eV via the formation of a negative molecular anion, which subsequently rapidly (0.1–1 fs) autoionizes to an excited electronic state of the neutral species. The electronic resonance excitation of H_2 by electrons has been reported in the experimental work of Kuyatt *et al* (1966), Weingartshofer *et al* (1970, 1975), Comer and Read (1971), Golden (1971), Sanche and Schulz (1972), Elston *et al* (1974), McGowan *et al* (1974), Schowengerdt and Golden (1975), Böse and Linder (1979) and have been extensively reviewed by Schulz (1973), and Hall and Read (1984).

Apart from excitation to the triplet state manifolds, excitation from the $X\ ^1\Sigma_g^+$ state to the singlet-gerade states such as $EF\ ^1\Sigma_g^+$ is the most important forbidden transition for molecular hydrogen. In contrast to triplet state excitation, which results in dissociation, predissociation and formation of metastable H_2 in the $v_j = 0$ level of the $c\ ^3\Pi_u^-$ state, the singlet-gerade excitation primarily leads to cascade transitions to the lower singlet-ungerade states, with subsequent transitions to the $X\ ^1\Sigma_g^+$ state, producing vacuum ultraviolet (VUV) emission. Under continuous electron impact excitation, H_2 VUV emission from cascade excitation of the singlet-ungerade states and direct (dipole-allowed) excitation are mixed into the same transitions. The presence of low-energy electrons in the atmospheres of the outer planets is determined by the measurable characteristics of the forbidden transitions to the singlet-ungerade Rydberg series. Furthermore, even at energies as high as 100–300 eV, a number of experimental studies have inferred that emission from cascade excitation is the dominant feature in certain portions of far-ultraviolet (FUV) wavelength regions (Ajello *et al* 1984, Liu *et al* 1995, Abgrall *et al* 1997, 1999).

The importance of the forbidden cascade excitation in the VUV emission spectra was realized in the early experimental investigations (Watson and Anderson 1977, Anderson *et al* 1977, Day *et al* 1979, Ajello *et al* 1982, 1984). These studies have shown that $EF\ ^1\Sigma_g^+$–$X\ ^1\Sigma_g^+$ excitation, followed by $EF\ ^1\Sigma_g^+$–$B\ ^1\Sigma_u^+$ cascade, is the dominant process leading to indirect excitation of the $np\sigma\ ^1\Sigma_u^+$ and $np\pi\ ^1\Pi_u$ states. The cascade excitation of the low v_j levels of the $B\ ^1\Sigma_u^+$ state is strong and readily recognizable. The cascade excitation of other levels of $B\ ^1\Sigma_u^+$, $C\ ^1\Pi_u$, $B'\ ^1\Sigma_u^+$ and $D\ ^1\Pi_u$ states, however, is weak and heavily mixed with the direct excitation process. It is only recently that the importance of excitations to the $EF\ ^1\Sigma_g^+$, $GK\ ^1\Sigma_g^+$, $H\bar{H}\ ^1\Sigma_g^+$, $I\ ^1\Pi_g$, $J\ ^1\Delta_g$, $O\ ^1\Sigma_g^+$ and $P\ ^1\Sigma_g^+$ states and their subsequent cascade emission to the $B\ ^1\Sigma_u^+$, $C\ ^1\Pi_u$, $B'\ ^1\Sigma_u^+$ and $D\ ^1\Pi_u$ states were revealed by time-resolved electron impact measurements in combination with theoretical modelling (Dziczek *et al* 2000, Liu *et al* 2002).

While many experimental investigations of excitation cross sections of the singlet-ungerade states have been reported (De Heer and Carrière 1971, Ajello *et al* 1984, Shemansky *et al* 1985a, Khakoo and Trajmar 1986, Liu *et al* 1998), the measurement of excitation functions for the singlet-gerade states such as EF $^1\Sigma_g^+$ has been sparse and insufficient. Watson and Anderson (1977), Anderson *et al* (1977) and Day *et al* (1979) have reported relative excitation functions for a limited number of rovibrational levels of the EF $^1\Sigma_g^+$, GK $^1\Sigma_g^+$, and H$\bar{\text{H}}$ $^1\Sigma_g^+$ states. The results of their studies have demonstrated that the shape of excitation function is quite complicated and shows a very significant dependence on rovibrational quantum numbers of the singlet-gerade states. Moreover, the dependence of the cross section on the excitation energy, even at or above 100 eV, generally does not show the expected dipole-forbidden $1/E$ relationship. Instead, the observed cross section decreases more slowly than $1/E$ as predicted by Born theory. Accurately modelling the excitation of the EF $^1\Sigma_g^+$ state, therefore, requires excitation function measurements over a large number of rovibrational levels.

An alternative way to obtain excitation functions of the EF $^1\Sigma_g^+$–X $^1\Sigma_g^+$ band system is by measuring the energy dependence of the cascade-excitation-dominated Lyman band emission intensities. A measurement of the energy dependence of the intensity for certain spectral features between 1332 and 1349 Å permits an approximate and indirect measurement of the EF $^1\Sigma_g^+$–X $^1\Sigma_g^+$ excitation function. The $v_j = 0$ level of the B $^1\Sigma_u^+$ state is primarily excited by the EF $^1\Sigma_g^+$–B $^1\Sigma_u^+$ cascade excitation (Liu *et al* 2002), and the emission features between 1332 and 1349 Å are dominated by the Lyman (0, 4) band. The derived functional form is an averaged excitation shape function and is thus more appropriately called 'effective' excitation function. A crude effective EF $^1\Sigma_g^+$–X $^1\Sigma_g^+$ shape function has been obtained in this way by Shemansky *et al* (1985a) by analysis of low-resolution (∼5 Å) spectra measured with steady-state excitation at several energies between 20 and 300 eV. The work of Shemansky *et al*, however, suffered from low spectral resolution, insufficient energy data points, and very crude theoretical modelling.

The first few members of the excited singlet-gerade states are $^1\Sigma_g^+$ series such as EF $^1\Sigma_g^+$ and GK $^1\Sigma_g^+$ states. These states are characterized by double-minimum potential energy curves that arise from the avoided crossings between the doubly excited $(2p\sigma_u)^2$ and singly excited $(2s\sigma_g)$ and $(3d\sigma_g)$ Rydberg states (Davidson 1961, Ross and Jungen 1987, 1994a, 1994b, Quadrelli *et al* 1990, Yu and Dressler 1994). The singlet-gerade series are known to be strongly coupled. Two principal theoretical methods have been used to calculate the excited singlet-gerade states. Ross and Jungen (1987, 1994a, 1994b, 1994c) have utilized multichannel quantum defect theory, whereas Dressler and Wolniewicz (1995), Quadrelli *et al* (1990), Wolniewicz (1996a, 1996b, 1998a, 1998b), Wolniewicz and Dressler (1977, 1994), and Yu and Dressler (1994) have carried out extensive *ab initio* calculations of the non-adiabatic coupling among the excited singlet-gerade states and obtained term energies by solving coupled equations. Both methods have revealed strong non-adiabatic interactions among these states and the energy level pattern cannot be accurately represented in terms of conventional rotation and vibration energy formulae. Glass-Maujean *et al* (1983, 1984a, 1984b) calculated band transition probabilities of the EF $^1\Sigma_g^+$–B $^1\Sigma_u^+$, EF $^1\Sigma_g^+$–C $^1\Pi_u$, GK $^1\Sigma_g^+$–B $^1\Sigma_u^+$, GK $^1\Sigma_g^+$–C $^1\Pi_u$, H$\bar{\text{H}}$ $^1\Sigma_g^+$–B $^1\Sigma_u^+$ and H$\bar{\text{H}}$ $^1\Sigma_g^+$–C $^1\Pi_u$ transitions and radiative lifetimes for $J_k = 1$ levels of the EF $^1\Sigma_g^+$, GK $^1\Sigma_g^+$ and H$\bar{\text{H}}$ $^1\Sigma_g^+$ states.

This paper reports an experimental measurement of the energy dependence of a single Lyman transition, the P(3) branch of the (0, 4) band, at a resolution of ∼180 mÅ over an energy range of 5–1800 eV. Four distinct excitation mechanisms that lead to the $J_j = 2$ and $v_j = 0$ level of the B $^1\Sigma_u^+$ are considered and modelled. The differences in threshold energy for each of the rovibrational excitations of the EF $^1\Sigma_g^+$–X $^1\Sigma_g^+$ band system are taken into

account. In addition to the observation of resonance excitation, this work also obtains a more accurate effective excitation function of the EF $^1\Sigma_g^+$–X $^1\Sigma_g^+$ system. Section 2 describes the experimental setup utilized to obtain the excitation function for the P(3) line of the (0, 4) Lyman band. Section 3 relates the measured excitation function to the four excitation processes which leads to the $J_j = 2$ and $v_j = 0$ level of the B $^1\Sigma_u^+$ state. It also provides a procedure to calculate the EF $^1\Sigma_g^+$–X $^1\Sigma_g^+$ Born cross section from the rotationally averaged form factor of Kolos *et al* (1982a). Section 4 describes data analysis in detail. Section 5 presents and discusses the results of analysis and compare them with previous results. Section 6 summarizes results obtained in this study.

2. Experiment

The experimental setup has been described in detail elsewhere (Liu *et al* 1995, 1998). The apparatus consists of a 3 m VUV spectrometer (Acton VM-523-SG) and an electron collision chamber. Electrons generated by heating a thoriated tungsten filament are collimated with an axially symmetric magnetic field of ∼100 G and accelerated to energies in the range from a few eV to ∼2000 eV with a full width at half maximum (FWHM) energy resolution of 0.5 ∼ 1 eV. The accelerated electrons collide with uniform density hydrogen gas (1×10^{-4}–5×10^{-6} Torr). Optical emission from electron-impact-excited H_2 was dispersed with the 3 m spectrometer equipped with a 1200 groove mm^{-1} grating coated with Al + MgF_2 and was detected with a channel electron multiplier (Galileo 4503) coated with CsI. A Faraday cup was used to minimize backscattered electrons and to monitor the electron beam current.

The excitation function measurement was a sum of multiple sweeps over the same energy range. Each scan commenced with the same initial electron beam energy and energy increment. After the photon emission signal was measured and accumulated over a certain period, corresponding to a set number of coulombs measured in the Faraday cup, the electron energy was raised by a selected increment and the signal was accumulated and recorded again. The process was repeated until the final energy was reached. Then, a new sweep with the same initial energy and increment was started. The recorded photon emission signal was added to the signal at respective energy obtained in the previous sweep. A measurement was completed when the predetermined number of scans was achieved. The accumulation time and energy increment were both uniform during the measurements. A typical measurement had peak counts of 2000 and consisted of 10–25 scans. Depending on the Faraday cup signal, the time interval lasted between 15 and 35 s. The energy increment was typically between 0.07 and 2.5 eV (see below). Electron beam currents used in the measurement were adjusted according to slit width and spectral intensities, and were generally between 10 and 70 μA.

The magnetically collimated electron gun suffered instabilities as described in James *et al* (1997) and Liu *et al* (1998). In addition to a possible secondary electron effect, the long-term stability of the gun filament presented an experimental problem. The performance of the electron gun filament changed significantly in 20–30 days. For a measurement performed around 10 days, experimental error arising from the instability of the electron gun and a possible secondary electron effect was estimated to be 8–13% by Liu *et al* (1998). In the present measurements, a small improvement in gun stability was more than offset by a larger gun aperture and beam current and a longer data acquisition time. As a result, the estimated experimental error is 9–16%, with the lower error limit applicable for data points below 300 eV and the higher limit for points above 1300 eV.

The data acquisition time for the weak transitions of the H_2 Lyman system could last as long as 20 days. To reduce the data acquisition time, excitation functions were measured with two separate sets of scans: one from ∼5 to ∼155 eV with a 0.07–0.3 eV energy increment, and

the other from ∼5 to 1800 eV with a ∼1.8 eV increment. The shape of the excitation function first rises sharply and declines rapidly to form a sharp well-defined local maximum between 11 and 13 eV. It rises again and reaches a global maximum at 40–60 eV, and then slowly decreases as the energy increases. The measurement from 5 to 155 eV with the smaller voltage step size yielded sufficient data points to characterize the shape of the low- to medium-energy regions, while the scan from 5 to 1800 eV permitted a measurement of the shape from medium- to high-energy region with less acquisition time. The FWHM of electron beam energy in the present experiment is 0.8–1 eV.

The P(3) line of the (0, 4) Lyman band (1342.257 Å) was selected for obtaining the excitation function of the EF $^1\Sigma_g^+$–X $^1\Sigma_g^+$ transition. The direct excitation of the $v_j = 0$ level of the B $^1\Sigma_u^+$ state is weak, while the cascade excitation is strong. More than 90% of the cascade emissions to the $v_j = 0$ of the B $^1\Sigma_u^+$ state, arising from the forbidden singlet-gerade excitation, are from the EF $^1\Sigma_g^+$ state (Liu *et al* 2002). Selection of the $v_j = 0$ level results in a great simplification of the data analysis. For excitation function measurement from the ∼5 to ∼155 eV with a fine voltage (0.073 28 eV) increment, the H_2 gas pressure was 10^{-4} Torr and the spectral window was from 1342.17 to 1342.35 Å. The small voltage increment, which is about 1/11 of electron energy beam width, was selected so that sufficient data points in the near-resonance and threshold regions are available for data analysis. For the scan from 5 to 1800 eV with a coarse (1.755 eV) increment, the spectral window was set from 1341.75 to 1342.75 Å. In addition, a lower gas pressure, 10^{-5} Torr, was used for the measurement between 5 and 1800 eV to reduce possible interference from secondary electrons. For a spectral window of 180 mÅ in the fine scan, interference from other transitions is negligible. For a window of 1 Å, interference from the nearby weak lines may be significant near the threshold energy region, but becomes negligible above 100 eV. The data acquisition time lasted 13 and 2 days, respectively, for the high-and low-resolution scans. Even with the long data collection time, the accumulated peak cross section count in the measured data is only ∼1800 counts (see solid curve of figure 1).

3. Theory

In this section, we relate the measured photon intensity to cross sections, and the theoretical Born cross section to the rotationally averaged form factor. Throughout the paper, we use indices i, j and k to denote appropriate levels of X $^1\Sigma_g^+$, singlet-ungerade and excited singlet-gerade states, respectively. When two sets of indices are required for singlet-ungerade states, we will use l as an additional index. We also neglect the minor discrepancy in electron kinetic energies for the laboratory and centre-of-mass frame. Thus, the excitation energy (E) denotes the kinetic energy of electron in the laboratory frame.

3.1. Electron-impact-induced emission

The steady-state volumetric photon emission rate (I) from continuous electron impact excitation is proportional to the excitation rate and emission branching ratio (Shemansky *et al* 1985a, Abgrall *et al* 1999):

$$I(v_j, v_i; J_j, J_i) = g(v_j; J_j)\frac{A(v_j, v_i; J_j, J_i)}{A(v_j; J_j)} \tag{1}$$

where v and J refer to vibrational and rotational quantum numbers, $A(v_j, v_i; J_j, J_i)$ is the Einstein spontaneous transition probability for emission from level (v_j, J_j) to level (v_i, J_i), and $A(v_j, J_j)$ is the total transition probability (including both discrete and continuum) for

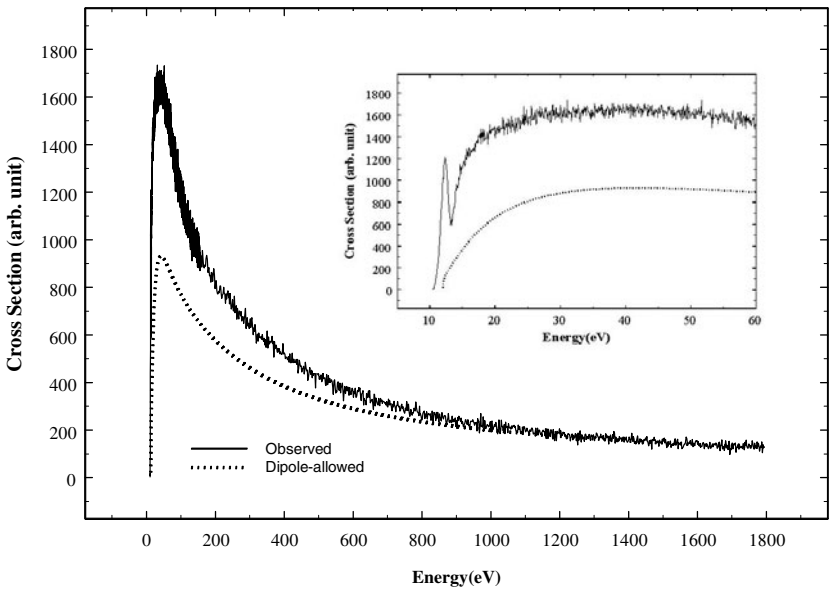

Figure 1. Observed excitation function as measured by the relative emission intensity of the $J_j = 2$ and $v_j = 0$ level of the B $^1\Sigma_u^+$ state (solid curve) of H_2. For comparison purposes, the emission cross section due to dipole-allowed excitation, both direct and indirect, is normalized to the observed value near 1780 eV, and is shown as a dotted curve. The difference between the solid and dotted curves provides a qualitative indication of the contribution from the dipole-forbidden singlet-gerade excitation, which, in the present case, is primarily from the EF $^1\Sigma_g^+$–X $^1\Sigma_g^+$ excitation. The inset shows the same traces in the low-energy region. The sharp peak near 12 eV is due to resonance excitation. Note that the relative magnitude of the dotted trace is actually much lower than the one shown. At 100 eV, for instance, the value of the dotted curve is only ∼13.4% of the corresponding value of the solid curve.

level (v_j, J_j); if a single index appears in the function definition, summation is implied over the missing index.

The excitation rate, $g(v_j; J_j)$, represents the sum of the rates for all excitations which lead to the $J_j = 2$ and $v_j = 0$ level of the B $^1\Sigma_u^+$ state. Four distinct excitation mechanisms are possible in the present study. H_2 can be excited directly to the $J_j = 2$ and $v_j = 0$ level of the B $^1\Sigma_u^+$ state from the X $^1\Sigma_g^+$ state via dipole-allowed P(3) and R(1) transitions. Its rate is denoted as g_{dd}. In addition, indirect excitation can take place by exciting to high-energy levels of the singlet-ungerade states (such as B′ $^1\Sigma_u^+$ and D $^1\Pi_u$) with subsequent cascade to the singlet-gerade states and finally to the $J_j = 2$ and $v_j = 0$ level of the B $^1\Sigma_u^+$ state. The cascade through singlet-gerade states is allowed by the electric dipole selection rule and is described as allowed indirect excitation. Its rate is represented by g_{id}. The third excitation pathway is via Feshbach resonance, when H_2 captures a slow electron to form H_2^- which autoionizes rapidly with the neutral molecule decaying to the low v_j levels of the B $^1\Sigma_u^+$ state. The contribution of resonance excitation can be substantial in the threshold energy region but negligibly small as the excitation energy increases above the first ionization potential. The resonance excitation rate is designated by g_{res}. The last pathway refers to the direct excitation from the X $^1\Sigma_g^+$ to the singlet-gerade states, from which molecular hydrogen decays to the lower singlet-ungerade states. Because the excitation is forbidden by the dipole selection rule, it will be called forbidden excitation in this paper and its rate is indicated by g_{fd}. The total excitation rate is thus given by

$$g(v_j; J_j) = g_{dd}(v_j; J_j) + g_{id}(v_j; J_j) + g_{res}(v_j; J_j) + g_{fd}(v_j; J_j). \tag{2}$$

The direct excitation rate, g_{dd}, is proportional to the population of molecules at the initial level, $N(v_i, J_i)$, the excitation cross section (σ), and the electron flux (F_e):

$$g_{dd}(v_j; J_j) = F_e \sum_i N_i \sigma(v_i, v_j; J_i, J_j) \tag{3}$$

where the cross section σ_{ij} is calculated from (Shemansky *et al* 1985a, 1985b)[5]

$$\frac{\sigma(v_i, v_j; J_i, J_j)}{\pi a_0^2} = 4 f(v_i, v_j; J_i, J_j) \frac{\text{Ryd}}{E_{ij}} \frac{\text{Ryd}}{E} \left[\frac{C_0}{C_7} \left(\frac{1}{X^2} - \frac{1}{X^3} \right) + \sum_{m=1}^{4} \frac{C_m}{C_7} (X-1) \exp(-mC_8 X) + \frac{C_5}{C_7} \left(1 - \frac{1}{X} \right) + \ln(X) \right] \tag{4}$$

where a_0 and Ryd are Bohr radius and Rydberg constant, respectively, $f(v_i, v_j; J_i, J_j)$ is the optical absorption oscillator strength, E_{ij} is the transition energy from (v_i, J_i) to (v_j, J_j), E is the impact energy, and $X = E/E_{ij}$. The coefficients C_m/C_7 ($m = 0$–5) and C_8 are determined by fitting the experimentally measured relative excitation function. For this work, C_m/C_7 ($m = 0$–5) and C_8 obtained by Liu *et al* (1998) for the Lyman band system of H_2 and oscillator strengths and transition probabilities calculated by Abgrall *et al* (1993a) (1993a, 1993b, 1993c, 1994 and 2000) are used.

The indirect dipole-allowed excitation represents the excitation to high-energy levels of the singlet-ungerade states l with subsequent cascade to excited singlet-gerade states k and finally to ungerade states j. The rate of excitation to state j can be written as

$$g_{id}(v_j; J_j) = F_e \sum_{l,k} \left(\sum_i N_i \sigma(v_i, v_l; J_i, J_l) \frac{A(v_l, v_k; J_l, J_k)}{A(v_l; J_l)} \frac{A(v_k, v_j; J_k, J_j)}{A(v_k; J_k)} \right) \tag{5}$$

where summation over indices l and k is subjected to the energy constraint $E_l > E_k > E_j$.

Resonance excitation of the low vibrational levels of the B $^1\Sigma_u^+$ state are thought to take place primarily via two temporary H_2^- states which are generally designated by 'a' and 'c' (Weingartshofer *et al* 1970, Sanche and Schulz 1972, Schulz 1973, Elston *et al* 1974, McGowan *et al* 1974). The vibrational frequencies of both 'a' and 'c' series are found to be ~0.3 eV. The resonance excitation of the B $^1\Sigma_u^+$ state via the 'a' series is much stronger than that via the 'c' series (~0.1 eV above the 'a' series). The intrinsic energy widths of both 'a' and 'c' are very narrow. Weingartshofer *et al* (1970) has shown that the energy width for the 'a' series vibrational bands is 40 meV (FWHM). *Ab initio* calculations by Stibbe and Tennyson (1998) obtained widths of 19–43 meV and 4–6 meV for the 'a' and 'c' series, respectively, for internuclear distance in the range 2.2–3.0 a_0. Because the energy resolution of the present electron beam is very broad (0.8–1.0 eV), it is not possible to resolve individual vibrational transitions between the anion and neutral states. We, therefore, represent the resonance excitation using a single Gaussian instrumental function for the differential resonance excitation profile:

$$g_{res}(v_j; J_j) = F_e \sum_i N_i \int_{E_1}^{E_2} A \exp[-B(E - E_0)^2] \, \mathrm{d}E \tag{6}$$

where A, B and E_0 are the parameters to be determined from experimental data, and E is an excitation energy. Based on the appearance of measured data, the integration limits, E_1 and E_2, are selected to be 9.5 and 16.5 eV, respectively.

[5] In Shemansky *et al* (1985a), (1985b), the collision strength parameter, C_7, relates to the optical absorption oscillator strength f_{ij} by

$$C_7 = \frac{4\pi a_0^2 (2J_i + 1)\text{Ryd}}{E_{ij}} f(v_i, v_j; J_i, J_j).$$

The last excitation mechanism arises from dipole-forbidden excitation to the singlet-gerade states, followed by cascade emission to the lower B $^1\Sigma_u^+$ state. Time-resolved measurements in combination with theoretical modelling by Liu *et al* (2002) have shown the importance of cascade excitation of the singlet-ungerade states via at least six states, EF $^1\Sigma_g^+$, GK $^1\Sigma_g^+$, H$\bar{\text{H}}$ $^1\Sigma_g^+$, I $^1\Pi_g$, J $^1\Delta_g$ and O $^1\Sigma_g^+$. However, for the cascade emission arising from dipole-forbidden excitations, the work of Liu *et al* (2002) has shown that the EF $^1\Sigma_g^+$–B $^1\Sigma_u^+$ cascade accounts for more than 90% of the total singlet-gerade cascade excitation to the $v_j = 0$ level of the B $^1\Sigma_u^+$ state. In this analysis, we assume that all the dipole-forbidden cascade excitation of the $v_j = 0$ level arises from the EF $^1\Sigma_g^+$–X $^1\Sigma_g^+$ excitation:

$$g_{fd}(v_j; J_j) = F_e \sum_{k=EF} \left(\sum_i N_i \sigma(v_i, v_k; J_i, J_k) \right) \frac{A(v_k, v_j; J_k, J_j)}{A(v_k; J_k)}. \tag{7}$$

Following Liu *et al* (2002), we express the cross section, σ_{ik}, as a product of electronic (F_{ik}), vibrational ($Q_{v,v'}$) and rotational (S_r) terms:

$$\sigma(v_i, v_k; J_i, J_k) = F_{i,k}(X) Q_{v_i,v_k} S_r(J_i, J_k). \tag{8}$$

The vibrational term, $Q_{v,v'}$, can be considered as a Franck–Condon factor. In this study, however, we have utilized the effective Franck–Condon factors for Q-branch excitation for $Q_{v,v'}$. The rotational term, S_r, consisting of both isotropic and anisotropic terms, has been given by Abgrall *et al* (1999) as

$$S_r(J_i, J_k) = \beta \delta_{J_i,J_k} + (1-\beta) \left[\frac{3(J_k+1)(J_k+2)}{2(2J_k+3)(2J_k+5)} \delta_{J_i,J_k+2} + \frac{J_k(J_k+1)}{(2J_k-1)(2J_k+3)} \delta_{J_i,J_k} + \frac{3J_k(J_k-1)}{2(2J_k-1)(2J_k-3)} \delta_{J_i,J_k-2} \right] \tag{9}$$

where $\delta_{J,J'}$ is the Dirac δ function. The parameter β ($0 \leqslant \beta \leqslant 1$) measures the relative contribution of the isotropic and anisotropic terms. Experimental measurements and modelling have yielded values of 0.55 ± 0.1 and 0.7 ± 0.1 for β at 20 and 100 eV, respectively (Liu *et al* 2002, Abgrall *et al* 1999). For this work, we take $\beta = 0.6$ over all the measured energy range. Equation (9) is applicable for a Σ_g–Σ_g or Σ_u–Σ_u electronic excitation. Rotational terms for excitations such as Σ_g–Π_g and Σ_g–Δ_g have been given elsewhere (Liu *et al* 2002).

The electronic term, $F_{i,k}(X)$, of equation (8) is modelled as an excitation shape function which accounts for the energy dependence of the cross section. $F_{i,k}(X)$ can be represented in a set of collision parameter functional forms similar to equation (4). However, the dipole term, $C_7 \ln(X)$, vanishes for a transition such as EF $^1\Sigma_g^+$–X $^1\Sigma_g^+$ and the high-energy asymptotic is determined by the value of C_5. The excitation function form for the singlet-gerade state, analogous to equation (4), can be written as

$$\frac{F_{i,k}}{\pi a_0^2} = \frac{\text{Ryd}}{E} C_5 \left[\frac{C_0}{C_5} \left(\frac{1}{X^2} - \frac{1}{X^3} \right) + \sum_{m=1}^{4} \frac{C_m}{C_5} (X-1) \exp(-m C_8 X) + \left(1 - \frac{1}{X} \right) \right] \tag{10}$$

where, again, $X = E/E_{ik}$ and E_{ik} is the threshold energy for $(v_i, J_i) \rightarrow (v_k, J_k)$ excitation.

A nonlinear least-square fit of measured (relative) excitation function enables a determination of the value of parameter C_8 and C_m/C_5 ($m = 0$–4). A known cross section at a particular excitation energy permits a determination of the absolute value of C_5, and, then, those of C_m ($m = 0$–4). Alternatively, the absolute value of C_5 can be calculated theoretically. For instance, it can be obtained by a numerical integration of the generalized oscillator strength over the entire momentum transfer region, as indicated by equation (16) of section 3.2.

3.2. EF $^1\Sigma_g^+$–X $^1\Sigma_g^+$ *Born cross section*

The Born cross section, σ_{ik}, for excitation $i \rightarrow k$, is related to momentum transfer, K, and generalized oscillator strength, $f_{ik}(K)$, by (Inokuti 1971, McDaniel 1989)

$$\sigma_{ik} = \frac{2\pi e^4 m}{E\mu} \int_{K_{min}}^{K_{max}} \frac{f_{ik}(K)}{K E_{ik}} \, \mathrm{d}K \tag{11}$$

where e and m are elementary charge and mass of electron, respectively, and μ is reduced mass of the e + H_2 collision system. E and E_{ik} are collision and threshold energies, respectively. The integration limits are from $K_{min} = k_i - k_k$ to $K_{max} = k_i + k_k$, where k_i and k_k are the initial and final momentum of the molecule, respectively. By virtue of the Franck–Condon approximation, the generalized oscillator strength can be expressed as (Kolos *et al* 1982a)

$$f_{ik}(K) = \frac{K^2}{2} \omega_k E_{ik} Q_{ik} g_{ik}(K) \tag{12}$$

where ω_k denotes the electronic degeneracy of the state k. Q_{ik} is the Franck–Condon factor for transition $i \rightarrow k$, and $g_{ik}(K)$ is the rotationally averaged electronic form factor as defined by Kolos *et al* (1982a). Kolos *et al* (1982b, 1983) have further shown that the dependence of the electronic form factor on rotational quantum number is very small, and the use of the rotationally averaged form factor is appropriate. Kolos *et al* (1982a) have tabulated the product[6], $K^2 g_{ik}(K)/2$, for K from 0.001 to 20 au. In order to use the rotationally averaged form factor calculated by Kolos *et al* (1982a), we recast equation (11) in the form of a rovibrational excitation cross section as

$$\frac{\sigma(v_i, v_k; J_i, J_k)}{\pi a_0^2} = \frac{2m\mathrm{Ryd}}{\mu E} Q_{v_i, v_k} S_r(J_i, J_k) \int_{y_{min}}^{y_{max}} y g_{ik}(y) \, \mathrm{d}y \tag{13}$$

where the rotational term, $S_r(J_i, J_k)$, is given by equation (9). Finally, the dimensionless integration limits in equation (13) are given by

$$y_{min} = \frac{\mu}{m} \sqrt{\frac{E}{\mathrm{Ryd}}} \left(1 - \sqrt{1 - \frac{m}{\mu} \frac{1}{X}} \right) \tag{14}$$

$$y_{max} = \frac{\mu}{m} \sqrt{\frac{E}{\mathrm{Ryd}}} \left(1 + \sqrt{1 - \frac{m}{\mu} \frac{1}{X}} \right) \tag{15}$$

where $X = E/E_{ik}$.

We note that the collision strength parameter, C_5, defined in equation (10), under Born and Franck–Condon approximations, is given by

$$C_5 = \frac{2m}{\mu} \int_0^{\infty} y g_{ik}(y) \, \mathrm{d}y. \tag{16}$$

Using the rotationally averaged form factor, $g_{ik}(K)$ given by Kolos *et al* (1982a), we numerically integrated equation (13). For y from 0 to 20, the Born cross section from threshold to ~1250 eV can be obtained.

4. Data analysis

The first step in data analysis is calibration of the excitation energy scale. For the measurement in the 5–155 eV range with a fine energy increment, the absolute energy was calibrated with the

[6] The value of $K^2 g_{ik}(K)/2$ for $K = 3.5$ au in table 2 of Kolos *et al* (1982a) should be 0.3875×10^{-4}, not 0.3875×10^{-3}.

appearance potential of the atomic hydrogen Lyman α. The accuracy of calibration is estimated to be 0.6–0.7 eV. For the measurement from 5 to 1800 eV with a large energy increment, the energy scale was established by matching the relative shape of the excitation function to that of fine increment measurement in the region 16–150 eV. As noted elsewhere (Liu *et al* 1998), the accuracy of the shape matching is $\sim$1.5 eV.

After the energy scale is established, background subtraction and data merge are performed. The averaged count value from the data points below the threshold energy was taken as background noise and subtracted from the data. The fine-increment data was then merged with the large-increment data between 70 and 154 eV. The merged data consist of fine-increment data from $\sim$5 to 155 eV and the scaled large-increment data from 155 to 1800 eV.

The solid curve of figure 1 shows merged and background subtracted data. The dotted curve shows the sum of the dipole-allowed direct and indirect excitation rates (see below), normalized to the observed data near 1780 eV. The crude difference between the solid and dotted traces is a qualitative but unambiguous indicator of the presence of contribution from dipole-forbidden excitation of the singlet-gerade states. The sharp peak around 12 eV in the solid trace of inset of figure 1 arises from Feshbach resonance excitation.

The normalized dipole-allowed excitation rates to the $J_j = 2$ and $v_j = 0$ level of the $B\ ^1\Sigma_u^+$ state, defined as $g_{dd}/(F_eN)$ and $g_{id}/(F_eN)$, can be calculated by using the excitation function reported by Liu *et al* (1998) and transition probabilities calculated by Abgrall *et al* (1993a, 1993b, 1993c, 1994, 2000, 2003) and Liu *et al* (2002). For the dipole-allowed direct excitation, only two rotational transitions, R(1) and P(3) excitation from the $v_i = 0$ level of $X\ ^1\Sigma_g^+$ to $J_j = 2$ and $v_j = 0$ of the $B\ ^1\Sigma_u^+$, need to be considered since H_2 population at $v_i > 0$ levels is negligibly small at 300 K.

For the normalized dipole-allowed indirect excitation rate, $g_{id}/(F_eN)$, a large number of intermediate states are involved. In general, emission from a singlet-ungerade level to the excited singlet-gerade levels is much less favourable than to the $X\ ^1\Sigma_g^+$ state. In addition, the emission cross sections of the $np\sigma\ ^1\Sigma_u^+$ and $np\pi\ ^1\Pi_u$ Rydberg series decrease very rapidly with principal quantum number (n) because of the decrease of excitation cross section and the presence of dissociation, predissociation and autoionization. Recent experimental investigations by Jonin *et al* (2000) and Liu *et al* (2000) in the extreme ultraviolet (EUV) region have shown that emissions from $n \geqslant 4$ Ryd series to the $X\ ^1\Sigma_g^+$ state are very weak. We therefore consider the discrete rovibrational levels of the first four singlet-ungerade states, $B\ ^1\Sigma_u^+$, $C\ ^1\Pi_u$, $B'\ ^1\Sigma_u^+$ and $D\ ^1\Pi_u$ for l in equation (5). Excitation functions measured for Lyman and Werner bands by Liu *et al* (1998) are used for the $B'\ ^1\Sigma_u^+$–$X\ ^1\Sigma_g^+$ and $D\ ^1\Pi_u$–$X\ ^1\Sigma_g^+$ excitation. Oscillator strengths and transition probabilities calculated by Abgrall *et al* (1993a, 1993b, 1993c, 1994, 2000) are used to obtain absolute cross sections, σ_{il}. For the singlet-gerade states, we include the $EF\ ^1\Sigma_g^+$, $GK\ ^1\Sigma_g^+$, $H\bar{H}\ ^1\Sigma_g^+$, $I\ ^1\Pi_g$ and $J\ ^1\Delta_g$ state in summation of k in equation (5). The contribution from higher states such as $P\ ^1\Sigma_g^+$ and $O\ ^1\Sigma_g^+$ is presumably negligible because the dominant configurations at internuclear distance less than 1.1 Å for $P\ ^1\Sigma_g^+$ and $O\ ^1\Sigma_g^+$ are $4d\sigma_g$ and $4s\sigma_g$, respectively, and because the $P\ ^1\Sigma_g^+$ and $O\ ^1\Sigma_g^+$ must be populated by transitions from higher singlet-ungerade states. The transition probabilities of $B\ ^1\Sigma_u^+$, $C\ ^1\Pi_u$, $B'\ ^1\Sigma_u^+$ and $D\ ^1\Pi_u$–$EF\ ^1\Sigma_g^+$,$GK\ ^1\Sigma_g^+$, $H\bar{H}\ ^1\Sigma_g^+$, $I\ ^1\Pi_g$ and $J\ ^1\Delta_g$ reported recently (Liu *et al* 2002) were calculated by considering non-adiabatic coupling among the singlet-ungerade series. The couplings among the singlet-gerade states were neglected. This work utilizes the refined transition probabilities obtained by including non-adiabatic coupling among both gerade and ungerade series. Non-adiabatic coupling among the gerade states is based on the *ab initio* results of Quadrelli *et al* (1990) and Yu and Dressler (1994). The details of the calculation and results are described in a paper by Abgrall *et al* (2003).

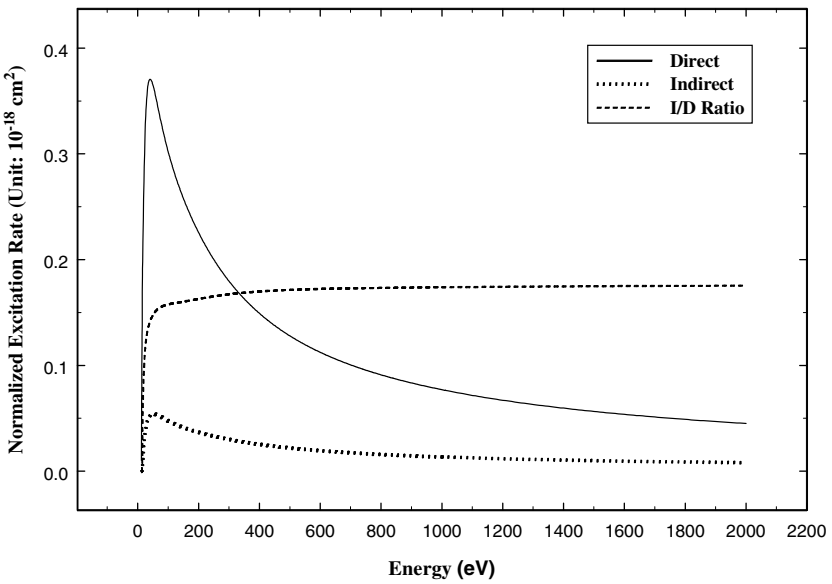

Figure 2. Normalized dipole-allowed direct (g_{dd}/F_eN) and dipole-allowed indirect (g_{id}/F_eN) excitation rates to $J_j = 2$ and $v_j = 0$ level of the B $^1\Sigma_u^+$ state. The direct rate is shown as a solid curve, and the indirect rate as a dotted curve. The ratio of indirect to direct rate, which has an asymptotic limit of ∼0.175, is displayed as a dashed curve. The temperature is assumed as 300 K. Excitation function reported by Liu *et al* (1998) and transition probabilities calculated by Abgrall *et al* (1993a, 1993b, 1993c, 1994, 2000, 2003) are utilized to obtain the rates (see text).

The calculated normalized excitation rates, g_{dd}/F_eN and g_{id}/F_eN, to the $J_j = 2$ and $v_j = 0$ level of the B $^1\Sigma_u^+$ state at 300 K, from threshold to 2000 eV, are shown as solid and dotted curves, respectively, in figure 2. The relative value of excitation rate, g_{id}/g_{dd}, is displayed as a dashed curve. It can be noted that the rise of the indirect rate lags behind that of the direct rate since the singlet-ungerade levels that contribute to the indirect excitation must have higher threshold energies than direct excitation. The effect of the differences in threshold energies on cross section essentially disappears over 500 eV. For this reason, the ratio, g_{id}/g_{dd}, rises from 0 in the threshold region to an asymptotic limit of ∼0.175 in the high energy region.

To make data more tractable for nonlinear least-squares analysis, the contribution from dipole-allowed (both direct and indirect) excitation is removed from the measured data to obtain an excitation function that is entirely due to forbidden and resonance excitations. Because cascade excitation contributes heavily to the $v_j = 0$ level of the B $^1\Sigma_u^+$ state, its contribution relative to that of direct excitation has been estimated in a number of experimental studies (Ajello *et al* 1984, 1988, Shemansky *et al* 1985a, Liu *et al* 1995, Abgrall *et al* 1997, 1999). For the $J_j = 2$ and $v_j = 0$ level, all these studies have consistently suggested a value of between 6.0 and 8.5 for the ratio $(g_{id} + g_{fd})/g_{dd}$ at 100 eV. In the present analysis, a ratio of 7.3, which is slightly above the mean, is adopted for 100 eV excitation energy. Coincidentally, the ratio of 7.3 also results in a correct asymptotic cross section limit $(1/E)$ for the dipole-forbidden portion of the excitation function up to the highest excitation energy in the present measurement, ∼1800 eV (see inset of figure 3). The excitation function for the $v_j = 0$ and $J_j = 2$ level that is entirely due to dipole-forbidden and resonance excitation is shown as a solid curve in figure 3.

A nonlinear least-squares program, based on the Marquard–Levenberg algorithm, is utilized to determine the value of C_m/C_5 ($m = 0$–4) and C_8. 170 rovibrational EF $^1\Sigma_g^+$–X $^1\Sigma_g^+$

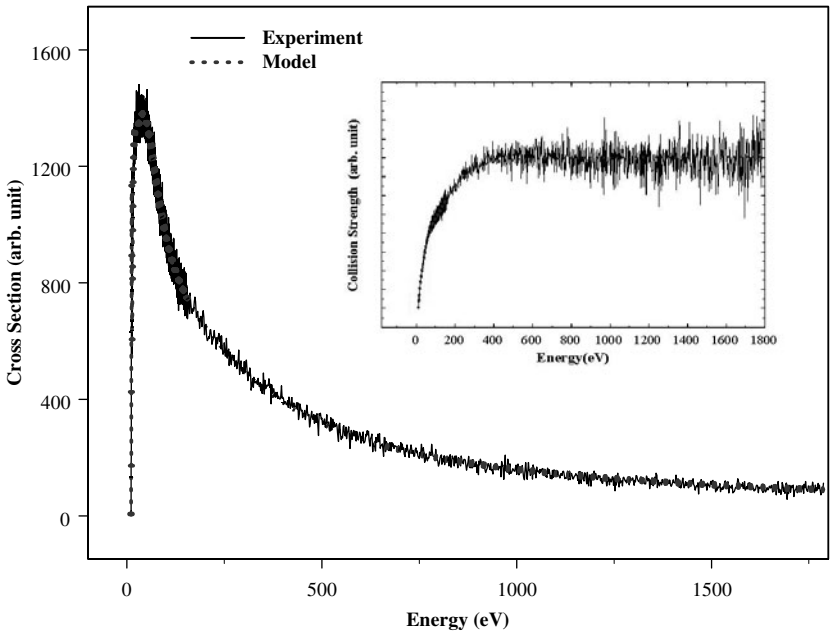

Figure 3. Comparison between the experimental (solid curve) and model (dotted curve) excitation function of H_2 EF $^1\Sigma_g^+$–X $^1\Sigma_g^+$ as measured via the P(3) branch of the (0, 4) Lyman band. Note that the contribution from both direct and indirect dipole-allowed excitations has been removed from the experimental trace. The inset shows the same sets of data in collision strength form. Also notice that the Born asymptotic limit (i.e. constant collision strength) is not reached until excitation energy is above ∼400 eV.

excitations are considered. Excitation threshold energies are calculated from experimental term values of EF $^1\Sigma_g^+$ and X $^1\Sigma_g^+$ states reported by Yu and Dressler (1994) and Dabrowski (1984). Apart from the difference in threshold energy, each of the 170 rovibronic excitations is assumed to have the same set of collision strength parameters C_m/C_5 ($m = 0$–4) and C_8. Figure 3 compares the resonance and EF $^1\Sigma_g^+$–X $^1\Sigma_g^+$ portion of the measured excitation function (solid line) with the model (dotted line) excitation function in both cross section and collision forms. Table 1 lists the determined collision strength parameters for both resonance and EF $^1\Sigma_g^+$–X $^1\Sigma_g^+$ excitation.

5. Discussion

5.1. Allowed excitation

The direct excitation from X $^1\Sigma_g^+$ to $J_j = 2$ and $v_j = 0$ level of the B $^1\Sigma_u^+$ state is calculated based on experimental measurements of Liu *et al* (1998) and transition probabilities of Abgrall *et al* (1993a, 1993b, 1993c, 1994, 2000). The accuracy of the direct excitation is probably higher than the accuracy of the present experimental data. Similarly, the applicability of the Lyman and Werner band excitation functions to B′ $^1\Sigma_u^+$–X $^1\Sigma_g^+$ and D $^1\Pi_u$–X $^1\Sigma_g^+$ and the accuracy of the B′ $^1\Sigma_u^+$–X $^1\Sigma_g^+$ and D $^1\Pi_u$–X $^1\Sigma_g^+$ transition probabilities have been verified in the experimental work of Jonin *et al* (2000). The transition probabilities of singlet-gerade–singlet-ungerade transitions are based on the recent *ab initio* calculation of Quadrelli *et al* (1990) and Dressler and Yu (1994). Their accuracy should be comparable to that of the

Table 1. Collision strength parameters for EF $^1\Sigma_g^+$–X $^1\Sigma_g^+$ band system and resonance excitation of the $J_j = 2$ and $v_j = 0$ of B $^1\Sigma_u^{+a,b}$.

Parameter	Value
C_0/C_5	0.504 902 67
C_1/C_5	−0.255 008 13
C_2/C_5	0.245 151 33
C_3/C_5	0.107 203 55
C_4/C_5	−1.723 674 6
C_8	0.209 837 77
A	0.070 42[c]
B	1.691
E_0	12.28

[a] See equations (6) and (10) for definition of parameters A, B, E_0 and C_m.
[b] An estimated value for C_5, 0.418 ± 0.104 with uncertainty of $\pm 25\%$, is obtained on the basis of experimental measurement of emission intensities from $v_j = 0$ and 1 level of the B $^1\Sigma_u^+$ state in FUV region (Liu *et al* 1995, Abgrall *et al* 1997, 1999).
[c] In unit of $\pi\, a_0^2$ eV^{-1}. The listed value is apparent as it is obtained not only without consideration of the selection rule on the change of rotational quantum numbers during resonance formation and autoionization processes, but also with an implicit assumption that molecular hydrogen at all J_i levels contributes to the resonance excitation of B $^1\Sigma_u^+(v_j = 0; J_j = 2)$ (see text).

D $^1\Pi_u$–X $^1\Sigma_g^+$ and B′ $^1\Sigma_u^+$–X $^1\Sigma_g^+$. Therefore, the uncertainties in allowed indirect excitation is primarily due to the number of intermediate states that are considered in the cascade process. As stated in section 4, consideration of B $^1\Sigma_u^+$, C $^1\Pi_u$, B′ $^1\Sigma_u^+$, D $^1\Pi_u$, EF $^1\Sigma_g^+$, GK $^1\Sigma_g^+$, HH̄ $^1\Sigma_g^+$, I $^1\Pi_g$, and J $^1\Delta_g$ states should be adequate, at least for the present analysis, for modelling of the allowed indirect excitation and emission process.

It is important to note that the g_{id}/g_{dd} ratio is temperature dependent. While only two rotation levels, $J_i = 1$ and 3, contribute to the g_{dd} of $J_j = 2$ and $v_j = 0$ level of the B $^1\Sigma_u^+$ state, three rotational levels, $J_i = 1$, 3, and 5, can populate the same B $^1\Sigma_u^+$ level by indirect excitation rate g_{id}. Thus, the g_{id}/g_{dd} ratio increases with temperature. Moreover, although the asymptotic limit for the relative rate, g_{id}/g_{dd}, for $J_j = 2$ and $v_j = 0$ level may appear quite large, it probably represents the upper limit of the relative rate for any singlet-ungerade levels. First, direct excitation from $v_i = 0$ of the X $^1\Sigma_g^+$ to $v_j = 0$ of the B $^1\Sigma_u^+$ state is inherently weak due to small Franck–Condon overlap integral. In addition, with exception of the $J_j = 0$ and 1 of the $v_j = 0$ level, the $J_j = 2$ level, being the third lowest rovibrational level of the singlet-ungerade state, can be populated by more higher singlet-gerade levels (and, indirectly, the ungerade levels) than any other singlet-ungerade levels.

5.2. Resonance excitation

Resonance excitation of the H_2 B $^1\Sigma_u^+$ state near the threshold energy region has been reported in many early experimental investigations (Kuyatt *et al* 1966, Heideman *et al* 1966, Weingartshofer *et al* 1970, Comer and Read 1971, Sanche and Schulz 1972, Elston *et al* 1974, McGowan *et al* 1974). Except in the work of McGowan *et al* (1974), who measured total optical emission intensities between 1410 and 1770 Å as a function of excitation energy, all other studies measured the electron energy loss of the scattered electron. All these energy loss spectra were measured with high-resolution electron beams. The present study is unique in that it has observed optical emission arising from resonance excitation of a single rovibrational level of the B $^1\Sigma_u^+$ state for the first time. However, due to the low resolution of electron beam energy (0.8–0.9 eV), resonance excitation from multiple channels appears only as a single resonance peak.

The parameters that characterize the resonance excitation, A, B and E_0, are also listed in table 1. While parameters B and E_0 are directly obtained from nonlinear least-squares analysis, only the relative value of A to C_5 is determined by the analysis. The absolute value of A is established by using the C_5 value derived in section 5.3.

The value of the B parameter listed in table 1 yields a FWHM of 1.28 eV for the resonance peak. Since the electron beam energy width is only 0.8–1.0 eV, the breadth of the resonance excitation function peak indicates the presence of multiple resonance excitation channels. Indeed, experimental studies of Kuyatt *et al* (1966), Heideman *et al* (1966), Weingartshofer *et al* (1970), Comer and Read (1971), Sanche and Schulz (1972) and Elston *et al* (1974) have shown that resonance excitation of the low v_j levels of the B $^1\Sigma_u^+$ primarily takes place via two H_2^- states, which are designated as 'a' and 'c' series, respectively. Based on theoretical calculations by Eliezer *et al* (1967) and angular distribution measurements by Weingartshofer *et al* (1970), Comer and Read (1971) have assigned a $^2\Sigma_g^+$ symmetry to the 'a' series. Early studies suggested that the 'a' state be viewed as a quasi-stationary compound state formed with an electron and neutral c $^3\Pi_u$ and a $^3\Sigma_g^+$ parent states (Comer and Read 1971, Elston *et al* 1974). More recent *ab initio R*-matrix scattering calculations by Stibbe and Tennyson (1997, 1998) have shown that the a $^3\Sigma_g^+$, EF $^1\Sigma_g^+$, c $^3\Pi_u$ and C $^1\Pi_u$ neutral states can all be viewed as parent states. The 'c' series is not as well understood as the 'a' series. Elston *et al* (1974) suggested the C $^1\Pi_u$ as the parent state of the 'c' series. Joyez *et al* (1973), on the other hand, assigned the c $^3\Pi_u$ state as the parent state. Similarly, disagreement exists about the electronic symmetry designation of the 'c' state: Sanche and Schulz (1972) designated it with $^2\Sigma_g^+$ configuration while Comer and Read (1971) and Joyez *et al* (1973) assigned it with $^2\Pi_u$ symmetry. Recent *ab initio* calculations by Stibbe and Tennyson (1998) confirmed that the 'c' series has a $^2\Pi_u$ symmetry with $^3\Sigma_g^+$, c $^3\Pi_u$ and EF $^1\Sigma_g^+$ as parent states. Stibbe and Tennyson (1998) also calculated ionization branching ratios of the 'a' series as a function of internuclear distance. At short internuclear distance ($\leqslant 1.6\ a_0$), the 'a' state primarily ionizes to the b $^3\Sigma_u^+$ state. Between 1.6 a_0 and 2.5 a_0, the X $^1\Sigma_g^+$ state is the major autoionization product. The branching ratio of the B $^1\Sigma_u^+$ state does not become significant until the distance is greater than 2.2 a_0 (Stibbe and Tennyson 1998). For resonance excitation of the B $^1\Sigma_u^+$ state, Elston *et al* (1974) have found that the contribution of the 'a' state is about 10 times greater than that of the 'c' state. At least nine vibrational bands (i.e. $v = 0$–8) have been observed for the 'a' series (Furlong and Newell 1995). The origin of the 'a' state is at 11.32 eV with a fundamental vibrational frequency of 0.3 eV. Of the nine vibrational levels, four ($v = 0$–3) are known to decay to the $v_j = 0$ level of the neutral B $^1\Sigma_u^+$ state (Weingartshofer *et al* 1970). Seven vibrational bands have been also seen for the 'c' state (origin at 11.4–11.5 eV) with a fundamental frequency of 0.3 eV. It is not known how many vibration levels of the 'c' state contribute to the resonance excitation B $^1\Sigma_u^+(v_j = 0)$. Since the $v = 0$ and 3 levels of the 'a' band are separated by $\sim$0.9 eV, we assume that the overall observed width of the resonance excitation channels, under the present experimental condition, is also approximately 0.9 eV. Since the energy width of the utilized electron beam is $\sim$0.9 eV, we can crudely estimate the width of observed resonance peak as $\sqrt{0.9^2 + 0.9^2}$ or 1.27 eV, consistent with the width implied by the value of parameter B in table 1.

The centre energy of the resonance peak, E_0, of table 1 is 12.28 ± 0.7 eV. Weingartshofer *et al* (1970) reported that the partial resonance excitation cross section from $v = 0$, 1, 2, and 3 levels of the 'a' anion state to the $v_j = 0$ level of B $^1\Sigma_u^+$ neutral state are 0.67×10^{-17}, 1.4×10^{-17}, 0.76×10^{-17} and 0.21×10^{-17} cm^2 respectively. Using their energy positions for $v = 0$–3 levels, the expected centre energy, based on the 'a' state alone, can be estimated to be 11.66 eV, lower than the observed centre energy, but within experimental error. Additional con-

siderations of resonance excitation from vibrational levels of the 'c' state and excitation of individual rotational levels are likely to yield a slightly higher expected centre energy than 11.66 eV.

The values of the parameters A, B and E_0 listed in table 1 lead to an estimated apparent resonance excitation cross section of $(8.1 \pm 3.2) \times 10^{-18}$ cm^2 for the $v_j = 0$ and $J_j = 2$ level of the B $^1\Sigma_u^+$ state. The value is apparent because rate equation (6) not only disregards the detailed mechanisms of resonance formation and autoionization, but also assumes that H_2 at all J_i levels contributes to the formation of H_2^- that eventually leads to the excitation of the B $^1\Sigma_u^+(v_j = 0;\ J_j = 2)$. If similar measurements and analyses for the $J_j = 0$, 4, and 6 levels had been performed at room temperature ($T = 300$ K), the resonance excitation cross section for the $v_j = 0$ level could be obtained by taking the ratio of the sum of the apparent cross sections for the $J_j = 0$, 2, 4, and 6 levels to the summed population fractions of H_2 at the odd J_i levels. In the absence of additional measurements, a crude estimate of the $v_j = 0$ resonance cross section is still possible. Assuming resonance excitation of the B $^1\Sigma_u^+(v_j = 0;\ J_j = 2)$ state exclusively arises from the 'a' $^2\Sigma_g^+$ state, it has been shown that only the incoming electrons with the even-order partial waves can contribute to the formation of the 'a' $^2\Sigma_g^+$ state and only the outgoing electrons with the odd-order partial waves in the autoionization can lead to the B $^1\Sigma_u^+$ state (Joyez *et al* 1973, Chang 1984). If the incoming electron is described by a pure s wave and outgoing electron by a pure pσ wave, the implied resonance excitation cross for the $v_j = 0$ level is $(1.7 \pm 0.7) \times 10^{-17}$ cm^2. On the other hand, if the incoming electron is described by a pure dσ wave and outgoing electron by a pure pσ wave, the implied resonance excitation cross is $(2.2 \pm 0.9) \times 10^{-17}$ cm^2 (Chang 1984). The total resonance cross section for the $v_j = 0$ level, reported by Weingartshofer *et al* (1970), is $(3.0 \pm 0.6) \times 10^{-17}$ cm^2. It appears that the dσ and pσ waves are more appropriate than the s and pσ waves. The dσ incoming partial wave and pσ outgoing wave are also consistent with the interpretation proposed by Chang (1975). It should be emphasized that the estimations are very crude as more than one partial wave can contribute to the resonance formation and autoionization process and interferences between these different order of waves and between resonance and non-resonance components are probable. Indeed, experimental work of Joyez *et al* (1973) has shown that both s and d waves contribute to the formation of the 'a' $^2\Sigma_g^+$ resonance state.

It should also be mentioned that the relatively large uncertainty (40%) in the apparent resonance cross section is primarily due to the relatively large energy width of the electron beam, which results in serious overlaps with the EF $^1\Sigma_g^+$–B $^1\Sigma_u^+$ cascade excitation and a weaker differential resonance profile. The uncertainty in the absolute energy scale also significantly affects the partition of the resonance and non-resonance components. It is important to note that while the rotational dependence of resonance is unknown and probably weak, the vibrational dependence is very significant. In general, the magnitude of the resonance excitation decreases with v_j of the B $^1\Sigma_u^+$ state (Weingartshofer *et al* 1970).

5.3. EF $^1\Sigma_g^+$–X $^1\Sigma_g^+$ *excitation function*

It is well known that some levels of the EF $^1\Sigma_g^+$ state are strongly coupled with other excited singlet-gerade states. The nonadiabatic wavefunction reported by Quadrelli *et al* (1990), for instance, shows that the $v_k = 0$–16 levels are essentially of pure ($\geqslant$98%) EF $^1\Sigma_g^+$ character while most of the $v_k = 17$–32 levels are strongly coupled with GK $^1\Sigma_g^+$, H$\bar{\text{H}}$ $^1\Sigma_g^+$, I $^1\Pi_g^+$ and J $^1\Delta_g^+$ states. In this analysis of the EF $^1\Sigma_g^+$–X $^1\Sigma_g^+$ excitation function, we have assumed all $J_k = 1$ and 3 levels have pure EF $^1\Sigma_g^+$ character. The assumption is necessitated by the nature of the experimental data where cascades from many rovibrational levels of the EF $^1\Sigma_g^+$ state (and, to a much lesser extent, the other singlet-gerade states) contribute to the excitation

of the B $^1\Sigma_u^+(v_j = 0;\ J_j = 2)$. Experimental determination of the effect of nonadiabatic coupling on the EF $^1\Sigma_g^+$–X $^1\Sigma_g^+$ excitation function is very difficult, if not impossible, without direct measurements of individual EF $^1\Sigma_g^+\rightarrow$ singlet-ungerade transitions. However, for this analysis, the error due to neglecting the nonadiabatic coupling is probably insignificant for three reasons. First, the probabilities of excitation from the $v_i = 0$ level of the X $^1\Sigma_g^+$ state to the coupled (i.e. $v_k = 17$–32) EF $^1\Sigma_g^+$ levels are very small. The sum of the Franck–Condon factors from $v_k = 0$ to 16 level amounts about 89% of the total EF $^1\Sigma_g^+$–X $^1\Sigma_g^+$ Franck–Condon factor. Additionally, emission branching ratios of many low v_k levels (inner well) to the $J_j = 2$ and $v_j = 0$ level are very large while those of the high v_k levels are very small. Finally, as in the case of Lyman and Werner bands (Liu *et al* 1998), the shape of excitation functions of the excited singlet-gerade states can be similar.

Excitation functions of some rovibrational levels of EF $^1\Sigma_g^+$ and other excited singlet-gerade states have been measured by Watson and Anderson (1977), Anderson *et al* (1977) and Day *et al* (1979) by monitoring the appropriate singlet-gerade $\rightarrow$B $^1\Sigma_u^+$ emission intensities as a function of excitation energy. All studies have reported two common important features of the singlet-gerade excitation. First, the shape of excitation function depends strongly on rovibrational quantum numbers of the singlet-gerade state. Excitation functions of some rovibrational levels are broad while others are very sharp. In addition, instead of the $1/E$ asymptote predicted by Born theory, almost all the measured cross sections show $E^{-0.6}$ to $E^{-0.85}$ energy dependence. The dependence persists even at 300 eV. Watson and Anderson (1977) initially explained the slower decline of cross sections for the low vibrational levels of the EF $^1\Sigma_g^+$ state by invoking cascade from the B$'$ $^1\Sigma_u^+$ state. However, the interpretation becomes problematic as subsequent measurements produced essentially similar energy dependence for higher vibration levels of the EF $^1\Sigma_g^+$ state and for GK $^1\Sigma_g^+$, H$\bar{\text{H}}$ $^1\Sigma_g^+$ and I $^1\Pi_g$ states, where the cascade contribution from the B$'$ $^1\Sigma_u^+$ and other singlet-ungerade levels is expected to be much less important.

This study differs from those of Watson and Anderson (1977), Anderson *et al* (1977) and Day *et al* (1979) in two aspects. First, this study measured the emission intensity of the P(3) line of the (0, 4) Lyman band. In addition, contributions from dipole-allowed excitations, direct or indirect, have been removed from the measured data. As a result, the solid line of figure 3 represents the emission due to the excitation from X $^1\Sigma_g^+$ directly to the singlet-gerade, or the EF $^1\Sigma_g^+$ state. Unlike the measurements reported by the previous studies, the solid trace in figure 3 is the sum of excitations to many rovibrational levels of the EF $^1\Sigma_g^+$ state weighted by their emission branching ratios to the B $^1\Sigma_u^+(v_j = 0;\ J_j = 2)$. Furthermore, each rovibrational excitation of the EF $^1\Sigma_g^+$–X $^1\Sigma_g^+$ band in the present analysis is assumed to have the same shape function even though Watson and Anderson (1977) have shown otherwise. Thus, the excitation function of table 1, as characterized by equation (10), is really an *effective* EF $^1\Sigma_g^+$–X $^1\Sigma_g^+$ excitation function that expresses the dipole-forbidden cascade excitation of B $^1\Sigma_u^+$ and C $^1\Pi_u$ states via the EF $^1\Sigma_g^+$ state.

One important characteristic of a dipole-forbidden excitation, as predicted by Born approximation, is that its collision strength has a constant asymptote. Operationally, the Born limit for these dipole-forbidden transitions is a constant collision strength. Most of the experimental measurements of the EF $^1\Sigma_g^+$, GK $^1\Sigma_g^+$, H$\bar{\text{H}}$ $^1\Sigma_g^+$ and I $^1\Pi_g$ states by Watson and Anderson (1977), Anderson *et al* (1977), and Day *et al* (1979) were made from $\sim$10 to 300 eV. It was believed that the starting energy of the Born limit for excitation from X $^1\Sigma_g^+$ to excited singlet-gerade state lies significantly below 300 eV. The $E^{-0.6}$ to $E^{-0.85}$ energy dependence of the cross section in the 15–300 eV region resulted in an overestimation of the cascade excitation

via singlet-ungerade states. The present study, however, has demonstrated that the beginning of the Born limit for the EF $^1\Sigma_g^+$–X $^1\Sigma_g^+$ excitation is around 400 eV (see inset of figure 3).

The starting energy of the EF $^1\Sigma_g^+$–X $^1\Sigma_g^+$ Born limit, 400 eV, is abnormally high. The Born limit for a number of molecular and atomic hydrogen transitions all seem to occur at much higher energies than those of other species. Liu *et al* (1998) have placed the Born asymptotic limit for dipole-allowed B $^1\Sigma_u^+$–X $^1\Sigma_g^+$ and C $^1\Pi_u$–X $^1\Sigma_g^+$ transitions at energy higher than 4000 eV. Similarly, James *et al* (1997) have obtained a starting point of Born limit at ∼1000 eV for atomic hydrogen 1s ^{2}S–2p ^{2}P excitation. In the case of both dipole- and spin-forbidden a $^3\Sigma_g^+$–X $^1\Sigma_g^+$ excitation of H_2, the asymptotic limit, where σ falls according to E^{-3}, is found to begin at slightly higher than 50 eV (Ajello and Shemansky 1993). In contrast, Born asymptotic limits for dipole-allowed 1 ^{1}S → 2 ^{1}P, 3 ^{1}P, and 4 ^{1}P excitations of helium all start at energy lower than 240 eV (Shemansky *et al* 1985b).

The collision strength parameters listed in table 1 permit a calculation of the relative cross section of the EF $^1\Sigma_g^+$ state at different excitation energies. Determination of the absolute cross section, however, requires a known EF $^1\Sigma_g^+$–X $^1\Sigma_g^+$ state cross section at a specific energy. In this work, we establish the absolute cross section of the EF $^1\Sigma_g^+$ state by using indirect cascade 'experimental' results inferred from measurements in FUV region. As mentioned in section 1, cascade excitation for the low v_j levels of the B $^1\Sigma_u^+$ state via singlet-gerade excitation is very strong. The intensity pattern due to the cascade excitation is drastically different from that of the direct excitation and, therefore, can be easily recognized (see, for instance, Liu *et al* 2002 and figure 4 of Abgrall *et al* 1999). As a result, a lower limit of the cascade excitation can be estimated by comparing model and observed spectra in a spectral region where the cascade excitation dominates. A number of experimental investigations in the FUV region, using different spectral resolutions, have estimated the cascade contribution to the discrete emission of $v_j = 0$–7 levels of the Lyman system to be 10–14% of the total direct excitation cross section at 100 eV impact energy (Ajello *et al* 1984, 1988, Shemansky *et al* 1985a, Liu *et al* 1995, Abgrall *et al* 1997). These estimates are made on the assumption that the cascade excitation to the other v_j levels of the B $^1\Sigma_u^+$ state and other singlet-ungerade states is negligible. This assumption is incorrect (Liu *et al* 2002). The high-resolution experimental spectrum (FWHM 0.136 Å) and direct excitation model Liu *et al* (1995), as refined in subsequent work of Abgrall *et al* (1997, 1999), Liu *et al* (1998) and Jonin *et al* (2000), are utilized for this purpose. The total cascade excitation cross section to the $v_j = 0$ and 1 levels of the B $^1\Sigma_u^+$ at 100 eV is found to be[7] $(1.75 \pm 0.40) \times 10^{-18}$ cm^2. The contribution to the $v_j = 0$ and 1 levels from dipole-allowed indirect excitation via higher levels of B $^1\Sigma_u^+$, C $^1\Pi_u$, B′ $^1\Sigma_u^+$ and D $^1\Pi_u$ state at the same excitation energy is calculated to be 0.17×10^{-18} cm^2. About 85–90% of the total singlet-gerade cascade excitation to the two vibrational levels is from the EF $^1\Sigma_g^+$ state

[7] Since only relative photoemission intensity was measured, any comparison of the observed and model spectra requires a normalization of the two spectra in certain wavelength regions where the contribution of cascade excitation is small. Moreover, if the VUV emission intensity pattern due to cascade from a singlet-gerade state were the same as or substantially similar to that of the direct excitation, the contribution from the singlet-gerade state would be very difficult, if not impossible, to recognize from the comparison without additional experimental investigations such as a time-resolved study or a direct measurement of singlet-gerade → singlet-ungerade transition. As mentioned, the modelling of time-resolved VUV spectrum by Liu *et al* (2002) has shown that EF $^1\Sigma_g^+$–B $^1\Sigma_u^+$ cascade excitation of the $v_j = 0$ and 1 levels of the B $^1\Sigma_u^+$ state is strong and its intensity pattern is drastically different from that of direct excitation. Cascade contributions from the GK $^1\Sigma_g^+$, H$\bar{\text{H}}$ $^1\Sigma_g^+$, I $^1\Pi_g$ and J $^1\Delta_g$ states are weaker and their intensity patterns are less different from the pattern of direct excitation than that of the EF $^1\Sigma_g^+$ state. Thus, even if the cascade excitation of the $v_j = 0$ and 1 levels of the B $^1\Sigma_u^+$ state via GK $^1\Sigma_g^+$, H$\bar{\text{H}}$ $^1\Sigma_g^+$, I $^1\Pi_g$, J $^1\Delta_g$ and other higher singlet-gerade states were more significant than estimated, it would not materially change the present EF $^1\Sigma_g^+$–X $^1\Sigma_g^+$ cross section value because their VUV emission intensity patterns combined together do not differ substantially from that of direct excitation.

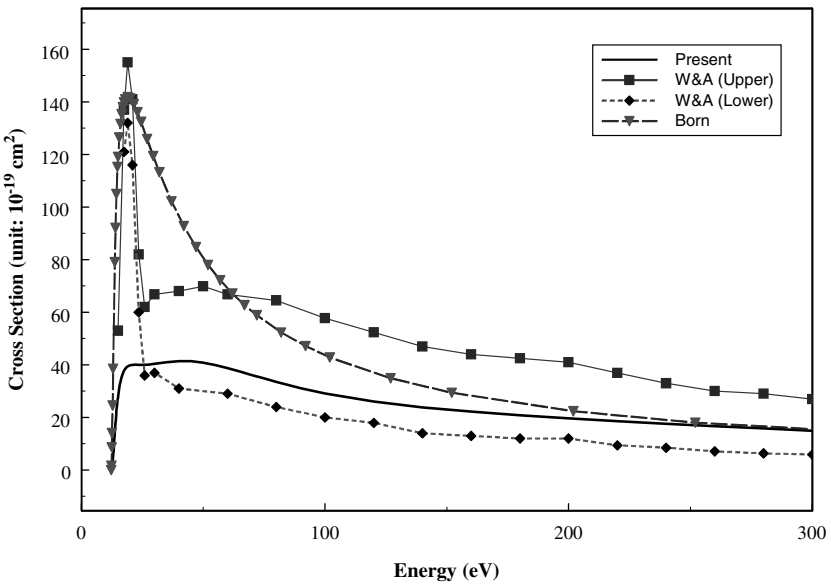

Figure 4. Comparison of the calculated EF $^1\Sigma_g^+$ Born cross section with various experimental cross sections. The Born cross section is displayed with triangles. The present experimental cross section, based on the ungerade coupled transition probabilities, is shown as a solid curve. The upper limit of the revised Watson and Anderson (1977) cross section is as squares while the lower limit is as diamonds.

(Liu *et al* 2002). The EF $^1\Sigma_g^+$–B $^1\Sigma_u^+$ partial emission cross section to $v_j = 0$ and 1 levels of the B $^1\Sigma_u^+$ state is, therefore, $(1.38 \pm 0.35) \times 10^{-18}$ cm^2 at 100 eV.

The partial EF $^1\Sigma_g^+$–B $^1\Sigma_u^+$ emission cross section to $v_j = 0$ and 1 levels at 100 eV, along with collision strength parameters in table 1, makes it possible to determine the absolute value of C_5 and calculate the EF $^1\Sigma_g^+$ excitation cross section over a wide energy range. The value of C_5 depends on the emission branching ratio to the $v_j = 0$ and 1 levels. The emission branching ratio, in turn, depends on the EF $^1\Sigma_g^+ \rightarrow$ singlet-ungerade transition probabilities. When the non-adiabatic coupling among the excited singlet-gerade states is neglected (but coupling among the singlet-ungerade states is taken into account), a value of $C_5 = 0.418 \pm 0.104$ is obtained. When the non-adiabatic coupling among the excited gerade states is considered[8], a slightly larger branching ratio to the B $^1\Sigma_u^+(v_j = 0;\ J_j = 2)$ is calculated (even though the EF $^1\Sigma_g^+$–C $^1\Pi_u$ branching ratio increases from 0.3 to 1.5%). The net result is that a slightly smaller value ($\sim$3%) of C_5 is required for non-adiabatic coupling. Because of the small difference, we will only use the cross section derived from $C_5 = 0.418 \pm 0.104$ for further discussion. The solid line in figure 4 shows the adiabatic EF $^1\Sigma_g^+$–X $^1\Sigma_g^+$ cross section and the last column of table 2 lists its numerical value.

[8] Two important points need to be stressed. First, since the non-adiabatic coupling among the excited singlet-gerade states is very strong, the adiabatic rovibronic designation, in some cases, has lost its conventional meaning and become ambiguous. The assignment of adiabatic state labels in the present work follows the designation by Quadrelli *et al* (1990) and Yu and Dressler (1994). Second, as the effect of non-adiabatic coupling among singlet-gerade states on individual rovibronic excitation shape function is not known, we have assumed that the coupling does not alter the shape. As far as the cascade excitation of the B $^1\Sigma_u^+(v_j = 0;\ J_j = 2)$ is concerned, the assumption makes little difference because the EF $^1\Sigma_g^+$ rovibrational levels that contribute heavily to the excitation are essentially free from the coupling. However, the validity of the assumption should be verified when considering the cross section of the 'eigen' EF $^1\Sigma_g^+$–X $^1\Sigma_g^+$ band system with $v_i > 0$.

Table 2. Comparison of H_2 EF $^1\Sigma_g^+$ cross sections (units in 10^{-19} cm^2).

E (eV)	Born[a]	Born[b]	*R*-matrix[c]	Exp[d]	Exp[e]	Exp[f]
15	119		77		53	28
16	132		95			33
17	138		119			37
17.5	140		125	121	137	38
19	142		137	132	155	39
20	141	139	139			40
21	140		137	116	141	40
23.5	135		155	60	82	40
26	128			36	62	40
30	118			37	67	40
40	96.4			31	68	41
50	80.6	78.4			70	41
60	69.1			29	67	39
70	60.3					36
80	53.5			24	65	34
100	43.6	42.6		20	58	29
120	36.8			18	52	26
140	31.8			14	47	24
160	28.0			13	44	22
180	25.0			12	42	21
200	22.6	22.1		12	41	20
220	20.6			9.4	37	19
240	19.0			8.5	33	18
260	17.5			7.1	30	17
280	16.3			6.4	29	16
300	15.3	14.8		5.9	27	15
400	11.5	11.2				12
500	9.23	8.96				9.6
600	7.71					8.0
700	6.62					6.9
800	5.80					6.1
900	5.16					5.4
1000	4.65	4.48				4.9
1100	4.23					4.4
1200	3.88					4.1

[a] Calculated in this work at $T = 300$ K.
[b] Calculated by Arrighini *et al* (1980a).
[c] From figure 10 of Branchett *et al* (1990).
[d] Lower limit of revised experimental value of Watson and Anderson (1977) who reported a 30% experimental uncertainty (see text).
[e] Upper limit of revised experimental value of Watson and Anderson (1977) (see text).
[f] This work, based on the transition probabilities of Liu *et al* (2002), which were calculated by considering non-adiabatic coupling among the singlet-ungerade states only. The experimental uncertainty is ±25%.

5.4. Comparison of EF $^1\Sigma_g^+$–X $^1\Sigma_g^+$ *cross sections*

Table 2 lists the present measured EF $^1\Sigma_g^+$–X $^1\Sigma_g^+$ cross section along with calculated and previously measured cross sections. Since some of listed cross sections require detailed explanations and revisions, we will discuss them individually.

We first compare our measured cross section with Born cross section calculated from the electronic form factor of Kolos *et al* (1982a), which is listed in the second column of table 2.

As can be seen from table 2 and figure 4, both sets of values track each other from 400 to 1200 eV with the experimental cross section being 4–5% higher. The agreement between the two sets of cross sections thus shows that the Born region of the EF $^1\Sigma_g^+$–X $^1\Sigma_g^+$ excitation begins at ∼400 eV. More importantly, the good agreement in the Born region also confirms the accuracy of experimental cross section. In the energy region from threshold to 300 eV, however, the calculated Born cross section is much greater than observation. The peak Born value, 142×10^{-19} cm^2, which occurs at ∼19 eV, is about 3.4 times greater than the maximum experimental cross section, 41.4×10^{-19} cm^2, which peaks at ∼40 eV. Moreover, the Born cross section also rises much faster than its experimental counterpart in the threshold energy region.

A comparison between experimental and calculated cross sections in the Born region can also be made with the values of C_5, which determines the magnitude of cross section in the asymptotic region. The experimental value of C_5 for the EF $^1\Sigma_g^+$–X $^1\Sigma_g^+$ band system, obtained in section 5.3, is 0.418 with an uncertainty of ±0.104. A theoretically calculated C_5 value can be obtained by numerically integrating the rotationally averaged electronic form factor via equation (16) from 0 to ∞. Since the data calculated by Kolos *et al* (1982a) only permits an integration from $y = 0.001$ to 20, we can obtain a lower limit of 0.4023 for the theoretical value of C_5, which agrees with the experimental value (0.418 ± 0.104) well within experimental uncertainty.

Table 2 also lists the cross section calculated by Arrighini *et al* (1980a) (third column) and Branchett *et al* (1990) (fourth column) and the revised experimental values of Watson and Anderson (1977) (fifth and sixth columns). The agreement between the present Born cross section and that calculated by Arrighini *et al* (1980a, 1980b) is very good, with the former being 2–3% larger than the latter. The EF $^1\Sigma_g^+$–X $^1\Sigma_g^+$ cross section calculated by Branchett *et al* (1990) with the *R*-matrix method clearly yields a better agreement with experimental values in the threshold energy region.

The fifth column of table 2 presents the revised EF $^1\Sigma_g^+$ state experimental cross section obtained by Watson and Anderson (1977). In general, the revised cross section is ∼20% larger than that originally reported. The cross section obtained by Watson and Anderson was based on the excitation function of the R(0) branch of the (2, 1) band for the E $^1\Sigma_g^+$-B $^1\Sigma_u^+$ system. The absolute emission cross section of this line at 200 eV was established to be $(46.8 \pm 14.0) \times 10^{-21}$ cm^2 by relative intensity measurement with the He II 4686 Å line. To obtain the apparent emission cross section for the $J_j = 1$ and $v_j = 2$ level of the E $^1\Sigma_g^+$ state, Watson and Anderson utilized an estimated inverse emission branch ratio, A(2;1)/A(2,1;1,0), of 4.2. However, a more accurate EF $^1\Sigma_g^+$–B $^1\Sigma_u^+$ transition probability calculation by Abgrall *et al* (2003) yielded a value of 5.76 for the inverse of the emission branching ratio. To convert the apparent emission cross section of the $J_j = 1$ and $v_j = 2$ level into the cross section of whole $v_j = 2$ level, it is necessary to know the steady-state population ratio of the $v_j = 2$ vibrational level to the $v_j = 2$ and $J_j = 1$ rovibrational level. Watson and Anderson obtained a population ratio of 5.7 at 300 K by using Born *dipole* approximation that involves P and R branch excitations. However, since the EF $^1\Sigma_g^+$–X $^1\Sigma_g^+$ excitation is dipole forbidden, it is *incorrect* to use the Born dipole approximation. In fact, the only ΔJ excitations allowed by symmetry are those with even integer change. In other words, the relative population should be calculated from equation (9). For $T = 300$ K and $\beta = 0.6$, the population ratio is obtained as 2.0, significantly below the value of 5.7 used by Watson and Anderson. Using the two revised values, the apparent 200 eV emission cross section of the $v_j = 2$ level of the E $^1\Sigma_g^+$ state is calculated to be $(5.3 \pm 1.6) \times 10^{-19}$ cm^2. The excitation function of the R(0) line for the (2, 1) band obtained by Watson and Anderson shows dual peaks. The first peak, at around 19 eV, is very sharp, while the second one, near ∼50 eV, is very broad. They attributed the sharp

peak to direct EF $^1\Sigma_g^+$–X $^1\Sigma_g^+$ excitation and the broad one to cascade excitation via the higher singlet-ungerade levels. By assuming that the direct EF $^1\Sigma_g^+$–X $^1\Sigma_g^+$ excitation cross section is inversely proportional to the excitation energy, they were able to separate the direct and cascade components by extending the fall of the first peak into the higher-energy region. They thus estimated that the direct excitation contributed only about 30% of the observed emission at 200 eV. The direct excitation cross section for the $v_E = 2$ level, based on their estimate, is thus $(1.6 \pm 0.5) \times 10^{-19}$ cm^2. The Franck–Condon factor for $Q(1)$ transition of the (2, 0) E $^1\Sigma_g^+$-X $^1\Sigma_g^+$ band is 0.13. The total EF $^1\Sigma_g^+$–X $^1\Sigma_g^+$ excitation cross section at 200 eV is, therefore, $(1.2 \pm 0.4) \times 10^{-18}$ cm^2, about 20% higher than the $(1.0 \pm 0.4) \times 10^{-18}$ originally reported by Watson and Anderson (1977). Cross sections listed in the fifth column are all uniformly scaled up by 20% from Watson and Anderson's original values. For the reasons outlined by Watson and Anderson (1977) and additional considerations given below, the cross section listed in the fifth column should be considered a lower limit of the EF $^1\Sigma_g^+$–X $^1\Sigma_g^+$ band system.

The cascade excitation of the $J_j = 1$ and $v_E = 2$ level at 200 eV, $(1.9 \pm 0.6) \times 10^{-19}$ cm^2, obtained based on the 30/70% direct/cascade partition by Watson and Anderson, appears to be abnormally large. The cascade excitation of the $J_j = 1$ and $v_E = 2$ level via dipole-allowed B $^1\Sigma_u^+$–X $^1\Sigma_g^+$, C $^1\Pi_u$–X $^1\Sigma_g^+$, B′ $^1\Sigma_u^+$–X $^1\Sigma_g^+$ and D $^1\Pi_u$–X $^1\Sigma_g^+$ transitions to this level can be calculated to be 2.4×10^{-20} cm^2 at 200 eV via equation (5) with minor changes. Likewise, consideration of higher states such as B″ $^1\Sigma_u^+$, D′ $^1\Pi_u$ and D″ $^1\Pi_u$ will not result in a cascade cross section anywhere close to $(1.9 \pm 0.6) \times 10^{-19}$ cm^2. This is because the total emission cross section of the B″ $^1\Sigma_u^+$, D′ $^1\Pi_u$ and D″ $^1\Pi_u$ states combined can be estimated to be $\sim 5.2 \times 10^{-19}$ cm^2 at 200 eV on the basis of experimental measurement and theoretical analysis of Jonin *et al* (2000) and Abgrall *et al* (2003). The latter work also showed that the total emission cross section from the B″ $^1\Sigma_u^+$ and D′ $^1\Pi_u$ states to the $J_j = 1$ and $v_E = 2$ level is slightly smaller than 4×10^{-21} cm^2. The cascade cross section is, therefore, 2.8×10^{-20} cm^2. Since the revised experimental apparent emission cross section for the $J_j = 1$ and $v_E = 2$ level is $(2.7 \pm 0.8) \times 10^{-19}$ cm^2, a more appropriate direct/cascade partition is 90/10%, instead of the 30/70% partition used by Watson and Anderson. Moreover, as indicated in figure 4, the present measurement strongly suggests that the Born limit for the H_2EF $^1\Sigma_g^+$–X $^1\Sigma_g^+$ excitation is not reached until $E \geqslant 400$ eV. It is questionable whether estimation of 200 eV direct excitation cross section based on an extrapolation of the sharp peak near 19 eV is appropriate.

We can obtain the upper limit of the EF $^1\Sigma_g^+$–X $^1\Sigma_g^+$ cross section based on the measurement of Watson and Anderson by assuming that the cascade excitation of the $J_j = 1$ and $v_E = 2$ level is entirely negligible. The upper limit of the revised Watson and Anderson EF $^1\Sigma_g^+$–X $^1\Sigma_g^+$ cross section is listed in the sixth column of table 2.

Figure 4 also compares the Born cross section with the revised experimental cross sections of Watson and Anderson. It can be seen that the calculation reproduces the revised Watson and Anderson cross section well in the first peak region. The calculated values are about 16, 8, and 21% greater than the lower limit Watson Anderson cross sections at 17.5, 19, and 21 eV, respectively. When compared with the values of the upper limit, the agreement is even better, with the largest difference only 9%. In comparison, the experimental uncertainty, originally given by Watson and Anderson, is ∼30%.

It should be mentioned that the EF $^1\Sigma_g^+$ cross section reported by Watson and Anderson (1977), as revised in this work, represents only a crude estimate. Excitation function measurements made with different rovibrational lines of the EF $^1\Sigma_g^+$–B $^1\Sigma_u^+$ band system show very different shape functions. While the cascade emission from the higher singlet-

ungerade levels may result in some variations in the measured shape function, the drastic shape function difference cannot be fully explained, as the energy dependence of the singlet-ungerade states is fairly well known from the experimental work of Liu *et al* (1998). Because of the significant variation of the shape function with rovibrational quantum number, the EF $^1\Sigma_g^+$–X $^1\Sigma_g^+$ excitation cross section obviously cannot be reliably obtained by a measurement of a few EF $^1\Sigma_g^+$–B $^1\Sigma_u^+$ transitions. Moreover, the direct excitation and cascade excitation via higher singlet-ungerade states is presumably very difficult to temporally separate in the experimental work of Watson and Anderson (1977), Anderson *et al* (1977) and Day *et al* (1979), as the lifetime of the singlet-ungerade states is only a few nanoseconds. Reliable separation of the direct and cascade components requires modelling with accurate transition probabilities of singlet-ungerade $\rightarrow$ singlet-gerade transitions and experiment excitation functions of the singlet-ungerade states.

Figure 4 shows that while the present experimental EF $^1\Sigma_g^+$–X $^1\Sigma_g^+$ cross section is within the upper and lower limits of Watson and Anderson (1977) in the region above 26 eV, the latter sets of cross sections are significantly greater than the former below 26 eV. The divergence can be explained in terms of the difference of methods by which the band cross sections are established. As explained, the present excitation function is an averaged shape function of many rovibrational EF $^1\Sigma_g^+$–X $^1\Sigma_g^+$ excitations that contribute to the excitation of a particular rovibrational level of the B $^1\Sigma_u^+$ state. The Watson and Anderson cross sections, on the other hand, are extrapolated from an emission measurement of the R(0) line of the (2, 1) band for E $^1\Sigma_g^+$–B $^1\Sigma_u^+$ transition, which happens to have a very sharp peak between 16 and 21 eV. Measurements of transitions such as R(0) and R(2) of the (5, 2) band of F $^1\Sigma_g^+$–B $^1\Sigma_u^+$ and P(4) of (3, 0) E $^1\Sigma_g^+$–B $^1\Sigma_u^+$ by Watson and Anderson, however, failed to show similar sharp peaks. Indeed, a significantly different band cross section between 16 and 23 eV would have been obtained if the P(4) line of the (3, 0) E $^1\Sigma_g^+$–B $^1\Sigma_u^+$ band had been used.

Finally, it should be mentioned that the present EF $^1\Sigma_g^+$–X $^1\Sigma_g^+$ excitation function also provides a much better description of energy dependence of the EF $^1\Sigma_g^+$–B $^1\Sigma_u^+$ cascade excitation than the previous one derived by Shemansky *et al* (1985a). As mentioned, the previous shape function was derived from an analysis of low-resolution ($\sim$5 Å) spectra at only a few energies between 20 and 300 eV. The dipole-allowed indirect excitation was not separated from the direct EF $^1\Sigma_g^+$–X $^1\Sigma_g^+$ excitation. As a result, a $C_7 \ln(X)$ term was retained in the functional form of Shemansky *et al*. For this reason, the two excitation functions have different asymptotic behaviour in the high-energy region. When both shape functions are normalized at $X = 8$ (i.e. $E \simeq 100$ eV), they track each other well in $X = 5$–25 ($E \simeq 60$–300 eV). The previous shape function, however, produces significantly larger cross sections in the region $X = 1.3$–3. Indeed, relative intensity measurements of the (0, 2) and (1, 2) to (8, 14) bands of Lyman system at excitation energies between 16 and 25 eV have shown that the previous excitation function overestimates the (0, 2) band intensity by as much as 180%. In contrast, the present effective function reproduces the relative intensity very well.

6. Conclusions

The electron impact emission function for the P(3) branch of the (0, 4) band of the Lyman system has been measured. Resonance excitation of a single rotational level has been observed for the first time. An apparent resonance excitation cross section of $(8.1 \pm 3.2) \times 10^{-18}$ cm^2 has been obtained for B $^1\Sigma_u^+$ ($v_j = 0$; $J_j = 2$). Due to the relatively large energy width of electron beam employed, this study is incapable of resolving various resonance excitation channels. Combined experimental and theoretical consideration enables partitioning of the

observed excitation function into resonance, dipole-allowed direct, dipole-allowed indirect and dipole-forbidden excitation components. A nonlinear least-squares analysis produces an effective excitation function for the EF $^1\Sigma_g^+$–X $^1\Sigma_g^+$ band system. A further experimental and theoretical consideration permits an estimation of the EF $^1\Sigma_g^+$–X $^1\Sigma_g^+$ excitation cross section over a wide energy region.

The dipole-forbidden component of the present measurement shows that the Born limit for the EF $^1\Sigma_g^+$–X $^1\Sigma_g^+$ excitation starts at ∼400 eV.

While the effective EF $^1\Sigma_g^+$–X $^1\Sigma_g^+$ excitation function neglects many fine details of each individual rovibrational excitation, its equivalency in the representation of the dipole-forbidden cascade excitation of B $^1\Sigma_u^+$ and C $^1\Pi_u$ states via the EF $^1\Sigma_g^+$ state makes it extremely useful in interpreting and modelling of electron-impact-induced emission spectrum of molecular hydrogen in the VUV region.

Acknowledgments

The analysis described in this paper was carried out at the University of Southern California and Meudon Observatory. The experimental data described in the paper were obtained by SMA and JA at Jet Propulsion Laboratory. XL and DS acknowledge grant support NASA OSS (NAG5-8939) to the University of Southern California. HA and ER wish to acknowledge the computing centre of Meudon Observatory SIO for computer facilities. The experimental part of the work was performed while SMA held a National Research Council Associate position at the Jet Propulsion Laboratory. JA acknowledges NASA Planetary Atmospheres, Astronomy/Space Physics and the Air Force Office of Scientific Research to the Jet Propulsion Laboratory.

References

Abgrall H, Roueff E and Drira I 2000 *Astron. Astrophys. Suppl. Ser.* **141** 297–300
Abgrall H, Roueff E, Launay F and Roncin J-Y 1994 *Can. J. Phys.* **72** 856–65
Abgrall H, Roueff E, Launay F, Roncin J-Y and Subtil J-L 1993a *J. Mol. Spectrosc.* **157** 512–23
Abgrall H, Roueff E, Launay F, Roncin J-Y and Subtil J-L 1993b *Astron. Astrophys. Suppl. Ser.* **101** 273–322
Abgrall H, Roueff E, Launay F, Roncin J-Y and Subtil J-L 1993c *Astron. Astrophys. Suppl. Ser.* **101** 323–62
Abgrall H, Roueff E, Liu X and Shemansky D E 1997 *Astrophys. J.* **481** 557–66
Abgrall H, Roueff E, Liu X and Shemansky D E 2003 in preparation
Abgrall H, Roueff E, Liu X, Shemansky D E and James G K 1999 *J. Phys. B: At. Mol. Opt. Phys.* **32** 3813–38
Ajello J M and Shemansky D E 1993 *Astrophys. J.* **407** 820–5
Ajello J M, Shemansky D E, Kwok T L and Yung Y L 1984 *Phys. Rev.* A **29** 636–53
Ajello J M, Srivastava S K and Yung Y L 1982 *Phys. Rev.* A **25** 2485–98
Ajello J M *et al* 1988 *Appl. Opt.* **27** 890–914
Ajello J M *et al* 1998 *J. Geophys. Res.* **103** 20125–148
Ajello J M *et al* 2001 *Icarus* **152** 101–17
Anderson R J, Watson J Jr and Sharpton F A 1977 *J. Opt. Soc. Am.* **67** 1641–3
Arrighini G P, Biondi F and Guidotti C 1980a *Mol. Phys.* **41** 1501–14
Arrighini G P, Biondi F, Guidotti C, Biagi A and Marinelli F 1980b *Chem. Phys.* **52** 133–41
Böse N and Linder F 1979 *J. Phys. B: At. Mol. Phys.* **12** 3805–17
Branchett S E, Tennyson J and Morgan L A 1990 *J. Phys. B: At. Mol. Opt. Phys.* **23** 4625–39
Chang E S 1975 *Phys. Rev.* A **12** 2399–40
Chang E S 1984 *J. Phys. B: At. Mol. Phys.* **17** 3341–51
Comer J and Read F H 1971 *J. Phys. B: At. Mol. Phys.* **4** 368–88
Dabrowski I 1984 *Can. J. Phys.* **62** 1639–64
Davidson E R 1961 *J. Chem. Phys.* **35** 1189–95
Day R L, Anderson R J and Sharpton F A 1979 *J. Chem. Phys.* **71** 3683–8
De Heer F J and Carrière J D 1971 *J. Chem. Phys.* **55** 3829–35

Dressler K and Wolniewicz L 1995 *Ber. Bunsenges. Phys. Chem.* **99** 246–50
Dziczek D, Ajello J M, James G K and Hansen D L 2000 *Phys. Rev.* A **61** 4702–6
Eliezer J, Taylor H S and Williams J K 1967 *J. Chem. Phys.* **47** 2165–77
Elston S B, Lawton S A and Pichanick F M 1974 *Phys. Rev.* A **10** 225–30
Furlong J M and Newell W R 1995 *J. Phys. B: At. Mol. Opt. Phys.* **28** 1851–8
Golden D E 1971 *Phys. Rev. Lett.* **27** 227–30
Glass-Maujean M, Quadrelli P and Dressler K 1984a *At. Data Nucl. Data Tables* **30** 273
Glass-Maujean M, Quadrelli P and Dressler K 1984b *J. Chem. Phys.* **80** 4355–62
Glass-Maujean M, Quadrelli P, Dressler K and Wolniewicz L 1983 *Phys. Rev.* A **28** 2868–75
Hall R I and Read F H 1984 *Electron–Molecule Collisions* ed I Shimamura and K Takayanagi (New York: Plenum)
Heideman H G M, Kuyatt C E and Chamberlain G E 1966 *J. Chem. Phys.* **44** 440–1
Ingersoll A, Vasavada A, Bolton S J, Klaasen K P, Anger C D and Little B 1998 *Icarus* **135** 251–64
Inokuti M 1971 *Rev. Mod. Phys.* **43** 297–347
James G K, Slevin J A, Shemansky D E, McConkey J W, Bray I, Dziczek D, Kanik I and Ajello J M 1997 *Phys. Rev.* A **55** 1069–87
Jonin C, Liu X, Ajello J M, James G K and Abgrall H 2000 *Astrophys. J. Suppl.* **129** 247–66
Joyez G, Comer J and Read F H 1973 *J. Phys. B: At. Mol. Phys.* **6** 2427–40
Khakoo M A and Trajmar S 1986 *Phys. Rev.* A **34** 146–56
Kolos W, Monkhorst H J and Szalewicz K 1982a *J. Chem. Phys.* **77** 1335–44
Kolos W, Monkhorst H J and Szalewicz K 1982b *J. Chem. Phys.* **77** 1323–34
Kolos W, Monkhorst H J and Szalewicz K 1983 *At. Data Nucl. Data Tables* **28** 239–63
Kuyatt C E, Simpson J A and Mielzarek S R 1966 *J. Chem. Phys.* **44** 437–9
Liu X, Ahmed S M, Multari R A, James G K and Ajello J M 1995 *Astrophys. J. Suppl.* **101** 375–99
Liu X, Shemansky D E, Abgrall H, Roueff E, Dziczek D, Hansen D L and Ajello J M 2002 *Astrophys J. Suppl.* **138** 229–45
Liu X, Shemansky D E, Ahmed S M, James G K and Ajello J M 1998 *J. Geophys. Res.* **103** 26739–58
Liu X, Shemansky D E, Ajello J M, Hansen D L, Jonin C and James G K 2000 *Astrophys. J. Suppl* **129** 267–80
McDaniel E W 1989 *Atomic Collisions: Electron and Photon Projectiles* (New York: Wiley)
McGowan J W, Williams J F and Meckbach W 1974 *Can. J. Phys.* **52** 2076–82
Pryor W R *et al* 1998 *J. Geophys. Res.* **103** 20149–58
Quadrelli P, Dressler K and Wolniewicz L 1990 *J. Chem. Phys.* **92** 7461–77 (and supplement tables, AIP document No. PAPS JCPA-92-7461-59)
Ross S C and Jungen C 1987 *Phys. Rev. Lett.* **59** 1297–30
Ross S C and Jungen C 1994a *Phys. Rev.* A **49** 4353–63
Ross S C and Jungen C 1994b *Phys. Rev.* A **49** 4364–77
Ross S C and Jungen C 1994c *Phys. Rev.* A **50** 4618–28
Sanche L and Schulz G J 1972 *Phys. Rev.* A **6** 69–86
Schowengerdt F D and Golden D E 1975 *Phys. Rev.* A **11** 160–4
Schulz G J 1973 *Rev. Mod. Phys.* **45** 423–86
Shemansky D E, Ajello J M and Hall D T 1985a *Astrophys. J.* **296** 765–73
Shemansky D E, Ajello J M, Hall D T and Franklin B 1985b *Astrophys. J.* **296** 774–83
Stibbe D T and Tennyson J 1997 *J. Phys. B: At. Mol. Opt. Phys.* **30** L301–7
Stibbe D T and Tennyson J 1998 *J. Phys. B: At. Mol. Opt. Phys.* **31** 815–44
Vasavada A R, Bouchez A H, Ingersoll A P, Little B and Anger C D 1999 *J. Geophys. Res.* **104** 27133–42
Watson J Jr and Anderson R J 1977 *J. Chem. Phys.* **66** 4025–30
Weingartshofer A, Clarke E M, Holmes J K and McGowan J Wm 1975 *J. Phys. B: At. Mol. Phys.* **8** 1552–69
Weingartshofer A, Ehrhardt H, Hermann V and Linder F 1970 *Phys. Rev.* A **2** 294–304
Wolniewicz L 1996a *J. Chem. Phys.* **105** 10691–5
Wolniewicz L 1996b *J Mol. Spectrosc.* **180** 398–401
Wolniewicz L 1998a *J. Chem. Phys.* **108** 1499–502
Wolniewicz L 1998b *J. Chem. Phys.* **109** 2254–6
Wolniewicz L and Dressler K 1977 *J. Mol. Spectrosc.* **67** 416–39
Wolniewicz L and Dressler K 1994 *J. Chem. Phys.* **100** 444–51
Yu S and Dressler K 1994 *J. Chem. Phys.* **101** 7692–706